Deployment analysis of a solar panel array as a demonstration of a new superelement formulation in multibody dynamics

M.H.M. Ellenbroek, J.P. Schilder
University of Twente, Faculty of Engineering Technology
P.O. Box 215, Enschede, The Netherlands
e-mail: **m.h.m.ellenbroek@utwente.nl**

Abstract
The floating frame of reference formulation is a commonly applied method in flexible multibody dynamics. The method requires Lagrange multipliers to enforce kinematic constraints between the bodies. To avoid the use of Lagrange multipliers, the authors have published a new formulation. This new formulation starts from the floating frame formulation. With a newly developed coordinate transformation, the floating frame degrees of freedom are converted into absolute nodal interface coordinates. Coupling of bodies in the interface points is similar as in the finite element method and the number of unknowns in the equations of motion are reduced to the degrees of freedom in a selected set of interface points. In this article, this new formulation is used to solve the transient deployment of a stacked solar panel array. Whereas earlier validations of the method were performed with two interface points per flexible body, the flexible bodies in this study have up to four interface points.

1 Introduction

In flexible multibody dynamics the geometric nonlinear motion of a system of flexible bodies is simulated. Floating frames are employed to introduce the possibility of large motion: Each body has its own floating frame which moves along with the body. The elastic deformation of the body is added as a local motion within the floating frame. Due to the superposition of a large rigid body motion and a local elastic motion, the coupling of bodies is not straightforward. Joints to couple bodies are introduced as kinematic constraint relations. In the end, this yields a set of complex differential-algebraic equations. Moreover, the number of degrees of freedom is extended with the so-called Lagrange multipliers.

In [1] the authors' introduced a new method that transforms the floating frame of reference equations into a form in which the absolute nodal coordinates are the unknown degrees of freedom. Absolute nodal coordinates enable a simple formulation of the joints between the different bodies. Moreover, it is even possible to implement joint relative coordinates as degrees of freedom in the system. In this way, the Lagrange multipliers are not needed anymore and a minimal set of degrees of freedom is used.

To show its potential, the method is used to simulate benchmarks where the bodies have two interface points. This is typically the case for beam-like structures. In this paper the method is applied to simulate the deployment of a solar array. The bodies then have at up to 4 interface points. For comparison, some results are compared to results obtained with the well-known multibody program MSC/ADAMS [6]. MSC/ADAMS is based on the standard floating frame of reference method.

The outline of this paper is as follows: In section 2 the floating frame of reference method is shortly explained. In section 3 the conversion of the floating frame equations to equations in terms of the absolute nodal coordinate is derived. The example of the solar array deployment is given in section 4. Simulation results are presented in section 5. Finally, the paper ends with the conclusions in section 6.

2 Floating frame of reference formulation

In the floating frame of reference formulation, the motion of a material point P on a body is described as the sum of the motion of a body reference frame and a local elastic displacement of P which is measured relatively to this body reference frame. See Figure 1, where as an example the body is a solar panel.

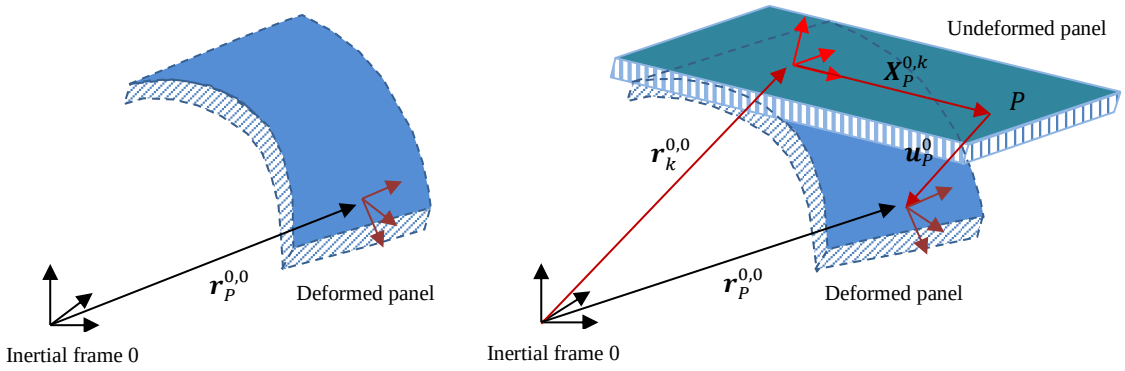

Figure 1: Kinematic description of a point P on a deformed solar panel.

The position of a material point P on the deformed panel is given by:

$$\boldsymbol{r}_P^{0,0} = \boldsymbol{r}_k^{0,0} + \boldsymbol{X}_P^{0,k} + \boldsymbol{u}_P^0 \tag{1}$$

In this, $\boldsymbol{r}_k^{0,0}$ is the position of the body reference frame expressed in the inertial reference frame. This frame is also referred to as the floating frame of panel k. $\boldsymbol{X}_P^{0,k}$ is the position of point P in the undeformed state of the body and it is expressed in the inertial reference frame. $\boldsymbol{u}_P^0$ is the elastic deformation of point P also expressed in the inertial reference frame.

Suppose that that orientation of the body reference frame k relative to the inertial frame 0 is given by the rotation matrix $\boldsymbol{R}_k^0$. This rotation matrix transforms the components of a vector expressed in frame k to the components of the vector in frame 0. With this, equation (1) can be reformulated as:

$$\boldsymbol{r}_P^{0,0} = \boldsymbol{r}_k^{0,0} + \boldsymbol{R}_k^0\left(\boldsymbol{X}_P^{k,k} + \boldsymbol{u}_P^k\right) \tag{2}$$

The local elastic displacement field $\boldsymbol{u}_P^k$ and the corresponding strains are assumed small and therefore the linear finite element method can be applied to relate the loads and the local nodal degrees:

$$\boldsymbol{M}^{FEM}\,\ddot{\boldsymbol{U}}^k + \boldsymbol{C}^{FEM}\,\dot{\boldsymbol{U}}^k + \boldsymbol{K}^{FEM}\,\boldsymbol{U}^k = \boldsymbol{L}^k \tag{3}$$

In this, $\boldsymbol{U}^k$ is the vector with nodal degrees of freedom of the finite element model, $\boldsymbol{M}^{FEM}$, $\boldsymbol{C}^{FEM}$ and $\boldsymbol{K}^{FEM}$ are the local system matrices and $\boldsymbol{L}^k$ is the externally applied load. The vector $\boldsymbol{U}^k$ and the local nodal degrees of freedom of a node located at the material points P_j are given by:

$$\boldsymbol{U}^k = \begin{bmatrix} \boldsymbol{U}_1^k \\ \vdots \\ \boldsymbol{U}_{N_k}^k \end{bmatrix},\ \boldsymbol{U}_j^k = \begin{bmatrix} \boldsymbol{u}_j^k \\ \boldsymbol{\theta}_j^k \end{bmatrix} \tag{4}$$

where $\boldsymbol{u}_j^k$ is the elastic displacement vector in P_j expressed in frame k and $\boldsymbol{\theta}_j^k$ is the elastic rotation vector in P_j expressed in frame k. The elastic rotation vector $\boldsymbol{\theta}_j^k$ defines the rotation matrix $\boldsymbol{R}_j^k$ orienting the frame attached in P_j relative to frame k. As the elastic deformation angles are small, this rotation matrix $\boldsymbol{R}_j^k$ can be obtained in several ways. For example assume that the elastic deformation angles are Bryant-Tate angles or components of a quaternion.

The following relation between the frame expressed in the inertial frame and the floating frame and the local elastic frame is valid:

$$\boldsymbol{R}_j^0 = \boldsymbol{R}_k^0 \boldsymbol{R}_j^k \tag{5}$$

Next consider the description of the elastic deformation field. To decrease computation time, the number of unknowns is reduced by selecting a number of interface points on the body and approximate the displacement field as a superposition of the corresponding well-known Craig-Bampton modes [3,4]. For example, identify on the solar panel in Figure 1 the interface points that interface with other panels. The following approximation is next introduced:

$$\boldsymbol{U}^k = [\boldsymbol{\Phi}_k]\boldsymbol{q}^k \tag{6}$$

where $\boldsymbol{q}^k$ is the vector with the local nodal degrees of freedom in the interface points. The material point where the floating frame is attached is also considered as an interface point, however, to obtain a suitable set of modes, the Craig-Bampton modes associated with the floating frame are not taken into account. This completes the geometric description.

From it the virtual displacements and the absolute acceleration in P can be obtained:

$$\delta\boldsymbol{r}_P^{0,0} = \delta\boldsymbol{r}_k^{0,0} + \delta\widetilde{\boldsymbol{\pi}}_k^{0,0}\boldsymbol{R}_k^0\left(\boldsymbol{X}_P^{k,k} + \boldsymbol{u}_P^k\right) + \boldsymbol{R}_k^0\left(\delta\boldsymbol{u}_P^k\right) \tag{7}$$

$$\ddot{\boldsymbol{r}}_P^{0,0} = \ddot{\boldsymbol{r}}_k^{0,0} + \dot{\widetilde{\boldsymbol{\omega}}}_k^{0,0}\boldsymbol{R}_k^0\left(\boldsymbol{X}_P^{k,k} + \boldsymbol{u}_P^k\right) + \widetilde{\boldsymbol{\omega}}_k^{0,0}\widetilde{\boldsymbol{\omega}}_k^{0,0}\boldsymbol{R}_k^0\left(\boldsymbol{X}_P^{k,k} + \boldsymbol{u}_P^k\right) + 2\widetilde{\boldsymbol{\omega}}_k^{0,0}\boldsymbol{R}_k^0\dot{\boldsymbol{u}}_P^k + \boldsymbol{R}_k^0\ddot{\boldsymbol{u}}_P^k \tag{8}$$

$\widetilde{\boldsymbol{\omega}}_k^{0,0}$ is a skew symmetric matrix by applying the tilde operator to the angular velocity $\boldsymbol{\omega}_k^{0,0}$ corresponding with the rotation matrix $\boldsymbol{R}_k^0$. The virtual elastic displacement is given by:

$$\delta\boldsymbol{U}^k = [\boldsymbol{\Phi}_k]\delta\boldsymbol{q}^k \tag{9}$$

From these expressions, after some mathematics is found that the virtual energy by the inertia loads of panel k is given by

$$\delta\boldsymbol{W}^{inertia} = \left[\left(\delta\boldsymbol{r}_k^{0,0}\right)^{\boldsymbol{T}} \quad \left(\delta\boldsymbol{\pi}_k^{0,0}\right)^{\boldsymbol{T}} \quad \left(\delta\boldsymbol{q}^k\right)^T\right]\left\{[\boldsymbol{M}_k]\begin{bmatrix}\ddot{\boldsymbol{r}}_k^{0,0}\\ \dot{\boldsymbol{\omega}}_k^{0,0}\\ \ddot{\boldsymbol{q}}^k\end{bmatrix} + [\boldsymbol{C}_k]\begin{bmatrix}\dot{\boldsymbol{r}}_k^{0,0}\\ \boldsymbol{\omega}_k^{0,0}\\ \dot{\boldsymbol{q}}^k\end{bmatrix}\right\} \tag{10}$$

The terms $\dot{\boldsymbol{r}}_k^{0,0}$ and $\boldsymbol{\omega}_k^{0,0}$ define the motion of the floating frame. They express the rigid body motion of panel k in the inertial frame. The elastic motion is noted locally by the motion of the selected interface points, i.e. $\boldsymbol{q}^k$. The inertia matrix $[\boldsymbol{M}_k]$ is given by:

$$[\boldsymbol{M}_k] = \begin{bmatrix}\boldsymbol{M}_k^{rig} & \boldsymbol{P}_k\\ \boldsymbol{P}_k^T & \boldsymbol{M}_k^{elas}\end{bmatrix} \tag{11}$$

In this, $\boldsymbol{M}_k^{rig} = \left(\boldsymbol{\Phi}_k^{rig}\right)^{\boldsymbol{T}}\boldsymbol{M}^{FEM}\boldsymbol{\Phi}_k^{rig}$ is the rigid body mass matrix where $\boldsymbol{\Phi}_k^{rig}$ are the 6 local rigid body vectors calculated relative to the floating frame, $\boldsymbol{P}_k = \left(\boldsymbol{\Phi}_k^{rig}\right)^{\boldsymbol{T}}\boldsymbol{M}^{FEM}\boldsymbol{\Phi}_k^{elas}$ is the modal participation matrix where $\boldsymbol{\Phi}_k^{elas}$ are the Craig-Bampton modes and $\boldsymbol{M}_k^{elas} = \left(\boldsymbol{\Phi}_k^{elas}\right)^{\boldsymbol{T}}\boldsymbol{M}^{FEM}\boldsymbol{\Phi}_k^{elas}$ is the reduced FEM mass matrix. Finally, $[\boldsymbol{C}_k]$ is a matrix with velocity terms. It is not expressed in more details in this paper.

The expression for the virtual elastic energy is given by:

$$\delta\boldsymbol{W}^{elastic} = \left(\delta\boldsymbol{q}^k\right)^T\boldsymbol{K}_k^{elas}\boldsymbol{q}^k \tag{12}$$

where $\boldsymbol{K}_k^{elas} = \left(\boldsymbol{\Phi}_k^{elas}\right)^{\boldsymbol{T}}\boldsymbol{K}^{FEM}\boldsymbol{\Phi}_k^{elas}$**.** The virtual energy from the damping loads are not considered in this paper.

In the floating frame formulation, the degrees of freedom of panel k are the absolute coordinates of the floating frame k and a set of local generalized coordinates. The absolute coordinates of the interface points are no degrees of freedom. As a consequence, the different solar panels can only be coupled by introducing kinematic constraints. Combining the expressions for the virtual energy and the just mentioned constraint relations, a set of differential-algebraic equations is finally obtained:

$$\begin{bmatrix} \boldsymbol{M} & \boldsymbol{\Phi} \\ \boldsymbol{\Phi}^T & \boldsymbol{0} \end{bmatrix} \begin{bmatrix} \ddot{\mathbf{q}} \\ \boldsymbol{\lambda} \end{bmatrix} = \begin{bmatrix} \boldsymbol{L} \\ \boldsymbol{\gamma} \end{bmatrix} \tag{13}$$

In this equation $\boldsymbol{M}$ is the system mass matrix assembled from the panel mass matrices, $\boldsymbol{\Phi}$ the Jacobian of the constraint equations and $\boldsymbol{L}$ are the sum of the internal loads and external loads (including also the velocity terms. $\boldsymbol{\gamma}$ is due to the second time derivative of the constraints. See for more information [3, 4,5].

3 Absolute nodal coordinates formulation

Due to the applied degrees of freedom in the floating frame of reference formulation a set of differential-algebraic equations is obtained. Numerically this might not be beneficial. In [1], a method is explained how the floating frame degrees of freedom can be transformed to only absolute nodal coordinates. The constraints to couple the different panels than become very straightforward and can be eliminated in the way it is done also in the standard finite element method. No Lagrange multipliers are needed anymore. A formulation in terms of a minimal set of degrees of freedom is derived. For an extensive explanation see [1,2].

The idea is to express the local Craig-Bampton degrees of freedom in the absolute nodal degrees of freedom in the interface points. The relevant expressions of the absolute nodal degrees of freedom in an interface point $\boldsymbol{P}_j$ are defined by:

$$\boldsymbol{q}_j^0 = \begin{bmatrix} \boldsymbol{r}_j^{0,0} \\ \boldsymbol{R}_j^0 \end{bmatrix}, \ \dot{\boldsymbol{q}}_j^0 = \begin{bmatrix} \dot{\boldsymbol{r}}_j^{0,0} \\ \boldsymbol{\omega}_j^{0,0} \end{bmatrix}, \ \delta\boldsymbol{q}_j^0 = \begin{bmatrix} \delta\boldsymbol{r}_j^{0,0} \\ \delta\boldsymbol{\pi}_j^{0,0} \end{bmatrix} \tag{14}$$

Note that they are related with help of (2) and (5) to the floating frame degrees of freedom and the local elastic degrees of freedom. Using these relations, it can be shown that for each interface point holds:

$$\begin{bmatrix} \delta\boldsymbol{r}_j^{0,0} \\ \delta\boldsymbol{\pi}_j^{0,0} \end{bmatrix} = \begin{bmatrix} \boldsymbol{I} & -\tilde{\boldsymbol{r}}_j^{0,k} \\ \boldsymbol{0} & \boldsymbol{I} \end{bmatrix} \begin{bmatrix} \delta\boldsymbol{r}_k^{0,0} \\ \delta\boldsymbol{\pi}_k^{0,0} \end{bmatrix} + \begin{bmatrix} \boldsymbol{R}_k^0 & \boldsymbol{0} \\ \boldsymbol{0} & \boldsymbol{R}_k^0 \end{bmatrix} \begin{bmatrix} \delta\boldsymbol{u}_j^k \\ \delta\boldsymbol{\theta}_j^k \end{bmatrix} \tag{15}$$

Next, assume that in contrast to the previous section, the floating frame is not an interface point. Then, no Craig-Bampton modes are associated with the floating frame and thus no modes are eliminated from the Craig-Bampton modes. This introduces a problem: The set of Craig-Bampton modes can describe a rigid body motion, which, however, is also described by the motion of the floating frame. The set of equations than cannot be solved uniquely. Additional constraints are required to remove the ambiguity. The interesting thing is that this provides a possibility to express the floating frame coordinates in the absolute nodal coordinates of the interface points. Collect from each Craig-Bampton mode the elastic displacements and orientations in the origin of the floating frame in a (6×1) vector and assemble these vectors in the matrix $[\boldsymbol{\Phi}_k]$. Remember that in the origin of the floating frame no interface point was defined:

$$[\boldsymbol{\Phi}_k] \equiv [\boldsymbol{\varphi}_1 \quad \cdots \quad \boldsymbol{\varphi}_{6N}] \tag{16}$$

N is the number of interface points. To remove the redundant rigid body motion from the set of Craig-Bampton modes require that the elastic degrees of freedom in the floating frame are zero:

$$[\boldsymbol{\Phi}_k]\boldsymbol{q}^k = \boldsymbol{0} \tag{17}$$

where $\boldsymbol{q}^k$ are the local elastic Craig-Bampton coordinates of all interface points. Taking the virtual change yields the following condition to be satisfied in order to remove the rigid body modes from the Craig-Bampton modes:

$$[\boldsymbol{\Phi}_k]\delta\boldsymbol{q}^k = \boldsymbol{0} \tag{18}$$

Note that equation (3.2) can be rewritten in compact form as:

$$\delta\boldsymbol{q}^k = [\bar{\boldsymbol{R}}_0^k]\delta\boldsymbol{q}_j^0 - [\boldsymbol{\Phi}_{rig}][\boldsymbol{R}_0^k]\delta\boldsymbol{q}_k^0 \tag{19}$$

Here $[\bar{\boldsymbol{R}}_0^k]$ is a $(6N \times 6N)$ block diagonal rotation matrix. $[\boldsymbol{\Phi}_{rig}]$ is the $(6N \times 6)$ matrix of rigid body modes of the deformed body. Substitution of (19) in (18) yields the incremental change of the floating frame

coordinates in terms of the incremental change of the absolute interface coordinates. This can be written in the following form, see [1]:

$$\delta \boldsymbol{q}_k^0 = \left[\mathbf{R}_k^0\right][\mathbf{Z}_k]\left[\bar{\mathbf{R}}_O^k\right]\delta \boldsymbol{q}^0, \quad [\mathbf{Z}_k] \equiv \left([\boldsymbol{\Phi}_k]\left[\boldsymbol{\Phi}_{rig}\right]\right)^{-1}[\boldsymbol{\Phi}_k] \tag{20}$$

When this results is back substituted in (15), an expression for the incremental change of the local interface coordinates in terms of the incremental change of the absolute interface coordinates is obtained

$$\delta \boldsymbol{q}^k = [\boldsymbol{T}_k]\left[\bar{\boldsymbol{R}}_0^k\right]\delta \boldsymbol{q}^0, \quad [\boldsymbol{T}_k] \equiv \mathbf{1} - \left[\boldsymbol{\Phi}_{rig}\right][\boldsymbol{Z}_k] \tag{21}$$

The resulting matrices in (20) and (21) provide the desired transformations to rewrite the equation of motion in the standard floating frame formulation of panel k in terms of the absolute interface coordinates:

$$\left[\bar{\boldsymbol{R}}_k^0\right]\boldsymbol{M}_k^{elas}\left[\bar{\boldsymbol{R}}_0^k\right]\ddot{\boldsymbol{q}}^0 + \left[\bar{\boldsymbol{R}}_k^0\right][\boldsymbol{T}_k]^T\boldsymbol{K}_k^{elas}\mathbf{q}^k = \boldsymbol{L}^0 \tag{22}$$

Note that the elastic loads are obtained from the local degrees of freedom. This is not a problem as during integration they are used in the right hand side of the equation of motion.

If the transformation is applied in all its details, the contributions of the inertia loads become complex. It includes a part depending on the accelerations of the absolute nodal degrees of freedom and a part depending on quadratic velocity forces. Often in the mass matrix this is completely ignored and the approximation as given in equation (22) is used. This was done when the new method described above was validated with benchmark problems using beam-like bodies. This approximation did not introduce significant errors. For that reason, the same approximation will be used in this work. Moreover, the inertia contribution introduced by quadratic velocity terms are neglected. It will be shown that this is a valid approximation for the application in this work, because angular velocities are relatively low.

4 Model of the demonstration solar array

A satellite relies on electric power provided by solar arrays. Usually, a solar array consists of a number of lightweight, CFRP honeycomb panels covered with solar cells. The solar array is connected to the sidewall of the satellite by means of a so-called yoke. During launch, the yoke and the panels are folded against the sidewall of the satellite. In this configuration, its volume is limited to a minimum and moreover, it can more easily withstand the severe launch loads. See Figure 2 for the Sentinel 1 satellite with two deployed arrays.

Once the satellite is in space, the array is deployed. The deployment is usually analyzed applying a multibody software tool like MSC/ADAMS. To test the newly developed superelement for bodies with more than 2 interface points, a demonstration model of a typical array is simulated.

Figure 2: Sentinel 1 satellite with two deployed solar arrays.

A solar array of the 'rigid' type is assembled from the following main subcomponents [8,9]:

- **Yoke**: this body is assembled from beam-like elements. It positions the deployed array relative to the satellite to avoid shading.
- **Solar panels**: The bodies are rectangular rigid aluminum honeycomb panels with CFRP face sheets, covered with GaAs solar cells.
- **Hinge**s: These are the joints between the satellite and the yoke, the yoke and the first panel and between the subsequent panels. Usually two hinges are mounted between the panels. Only between the satellite and the yoke one hinge is used. The hinges lock when they have opened over a certain angle. The hinge between the satellite and the yoke usually locks at 90 degrees and the other hinges at 180 degree.
- **Springs**: These are load providing elements mounted in the hinges. They force the array to open.
- **Synchronization system**: This passive control system takes care that the deployment of the angles is synchronized.
- **Damper**: Load providing element to control the angular velocities in the hinges. Usually it is mounted at the root hinge, i.e. the hinge between the satellite and the yoke. In the demonstration model used in this article, no damper is applied.

The geometry of the demonstration model is presented in figure 3. A more detailed description of the FEM model of the yoke and the panels are shown in figure 4 and figure 5 respectively.

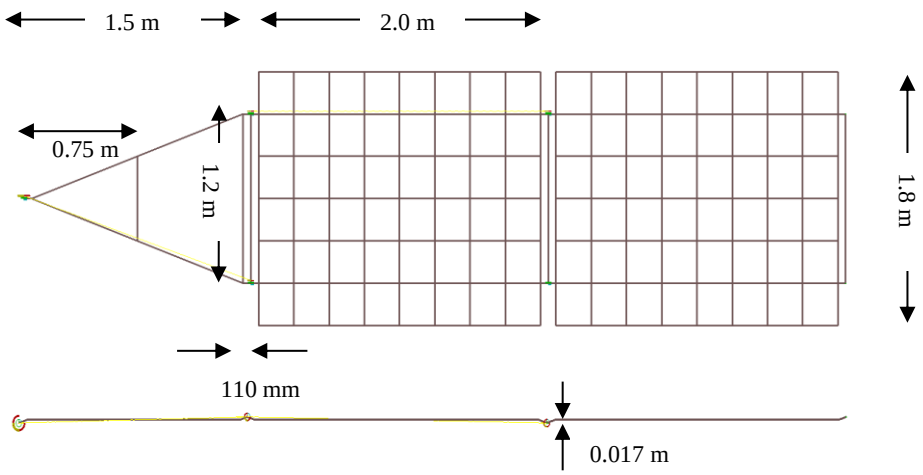

Figure 3: Geometry of the demonstration solar array.

The yoke is assembled from CBAR elements. In Figure 4, all black and gray dots are concentrated mass points. The red dot indicates where the floating frame in the new super element is chosen. All the yoke bar elements have the same properties. They are given in table 1in MSC/Nastran format [7].

Table 1: Bar properties used in the yoke model.

PBAR		10	5.0E-4	7.0E-8	7.0E-8	14.0E-8	0.0
MAT1		7.1+10		0.3			
CONM2			0.9				
	3.24E-4		3.24E-4			3.24E-4	

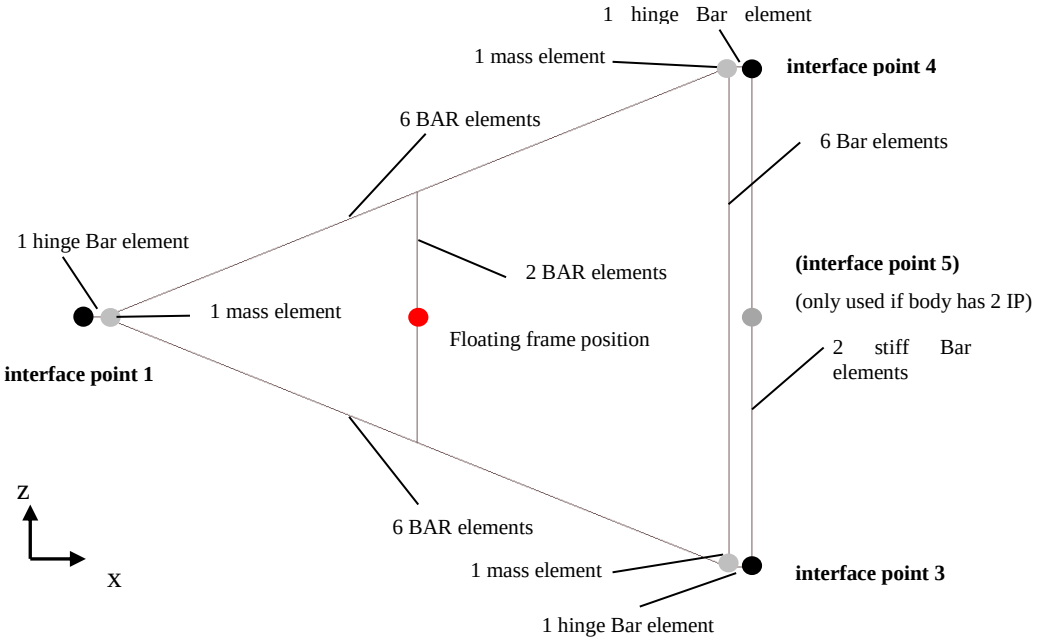

Figure 4: Overview of the yoke, using bar elements

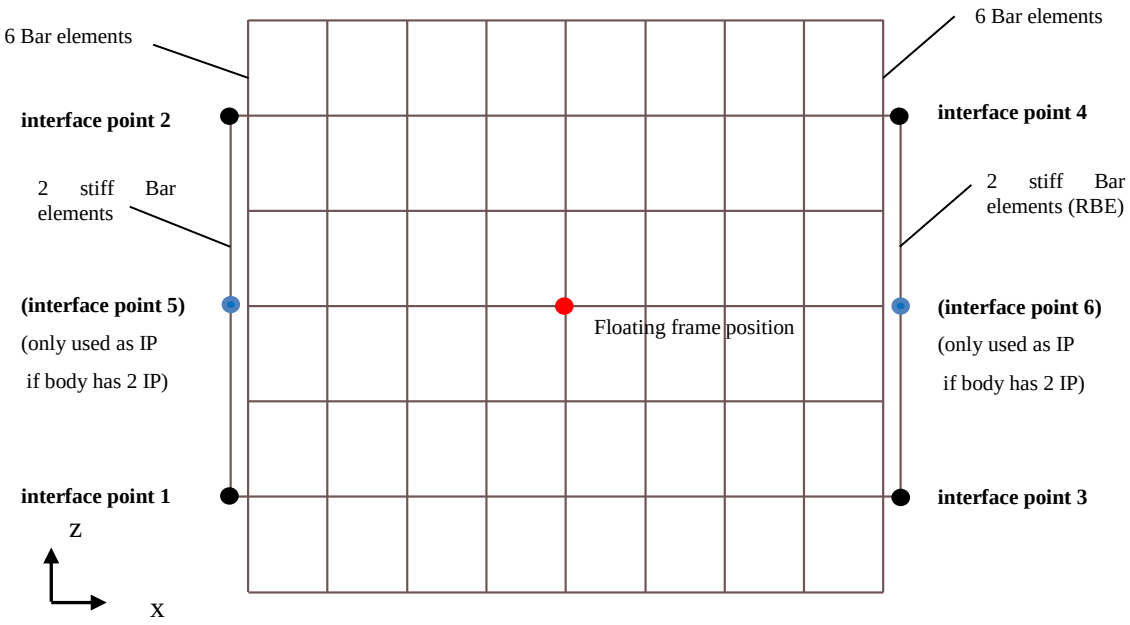

Figure 5: Overview of panel 1 and panel 2, using 16 CQUAD elements.

The panels are assembled from CQUAD4 elements. Along the edges with the hinges two edge members by means of CBAR elements are modelled. The hinge is modelled with a single CBAR element. In all dots but the blue ones concentrated masses are defined. The properties of the elements are given table 2 in MSC/NASTRAN format [7].

Table 2: Element properties used in the panel model..

PBAR		10	5.4E-4	7.0E-8	7.0E-8	14.0E-8	0.0
MAT1	10	7.1+10		0.3			
PSHELL		100	3.60-4	100	11200.	19.13	
MAT1	100	1.21E11		0.3			
CONM2			0.55				
	1.98E-4		1.98E-4			1.98E-4	

Two reduced models of the yoke are created. One is used to create a reduced multibody model of beam-like bodies with two interface points and one is used to demonstrate that the bodies can have any shape and more than two interface points. The interface points used to reduce the FEM models are:

- A beam-like model with two interface points, node 1 and node 5.
- A 3D model with three interface points: node 1, node 3 and node 4.

The models of the panels are reduced also in two ways:

- A beam-like model with two interface points, node 5 and node 6
- A 3D model with four interface points: node 1, node 2, node 3 and node 4.

These two multibody systems are shown below in Figure 6.

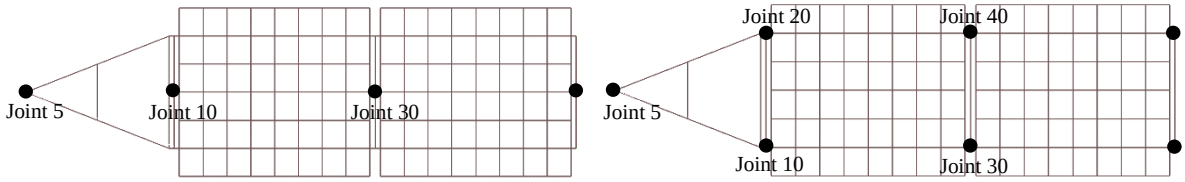

Figure 6: Multibody models of the solar array. Left: with two interface points per body, right: with more than two interface points per body. At these interface points, the bodies are connected by a revolute joint.

To force the array to deploy, torsional springs are mounted in the hinges. The torque varies linearly with the angle. The values used in the demonstration model are given in table 3. If the angles reach a certain value, the hinges lock. This is modelled by activating a spring in the model. In case of the beam-like multibody model, the values for the torque setting and the lock stiffness are doubled at certain hingelines to compensate for one hinge less.

Table 3: Hingeline lock-stiffness and the linear distributed deployment torque.

Hingeline	Lock stiffness Nm/rad	Configuration	Angle (degrees)	Torsion spring torque (Nm)
1	5000	Stowed	0	13
		Deployed	90	8
2	1500	Stowed	0	9
		Deployed	180	6
3	1500	Stowed	0	9
		Deployed	180	6

To enforce that each hinge always opens, the moment provided by the torsion spring compensates for all friction with a certain safety margin. Due to this safe torque setting, the deployment is not tuned for a controlled deployment. The array may enter even forbidden regions. This is unwanted. Therefore a system is implemented that synchronizes the deployment motion. A passive system that is often used is based on cables and pulleys. It is schematically shown in figure 7.

The figure shows three panels, two hingelines (HL) with two pulleys and two cables. The system intends to synchronize both angles. Each cable end is connected to a pulley mounted in a hinge. The pulley is fixed to a panel. In the first picture, the right (lower) pulley is fixed to the bottom panel and the left (upper) pulley is connected to the top panel. The cables are guided along the intermediate (second) panel. The radius of the pulley is tuned. When the deployment angle of both hinges is the same, the radius of both pulleys is the same. However, in case the cable runs along the yoke, then the pulley radius in hingeline 1, attached to the satellite (bottom panel is then the satellite), has two times the radius of the pulley in hingeline 2 and is attached to panel 1 (satellite). The explanation of the system is that, if both hinges open synchronized, the cable does not stretch and no additional moment is applied. However, when the angles are different, the cable is stretched and a corrective moment is applied. As a cable can only stretch two cables are required as shown in the figure. Depending on the difference in angles, one of the two cables is stretched. Because the stretching depends linearly on the error in angles, the applied moment is linear with the error in the angles. Such a system of pulleys and cables can be characterized as a passive controller. Properties of the synchronization system are given in table 4.

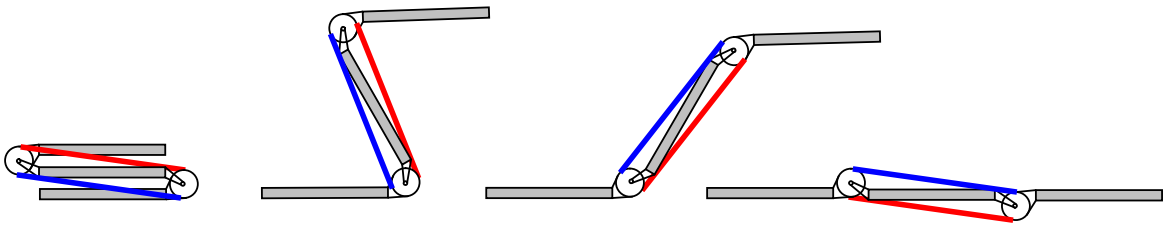

Figure 7: Explanation of the Synchronization system, including cables and pulleys.

Table 4: Properties of the synchronization system.

		Satellite HL1 pulley		HL 2 pulley		HL 3 pulley
	AE	Satellite	Yoke	Panel 1	Panel 2	Panel 3
Cable behind yoke	2.05E5 N/m	40			20	
Cable behind Panel 1	2.05E5 N/m		20			20

5 Simulation results of the demonstration solar array

5.1 Unsynchronized deployment

For the unsynchronized case, the deployment angles of the demonstration model during the deployment are shown in figure 8 and figure 9. In figure 8, the multibody model is the beam-like model with two interface points per body. For such a configuration it has already been shown that the new algorithm provides correct answers. For comparison, the results are compared with results from the MSC/ADAM model. However, since no ADAMS model with only two interface points per body was available, the ADAMS results hold for the 3D model with more than two interface points. The deployment angles and the torque after locking are shown in figure 8. The angles show that the deployment is not synchronized, i.e. the moment of locking differs per joint. Interesting to note is that the new method and ADAMS compare very good before the hinges lock. After locking of the second hinge a difference is observed. A plausible reason might be that locking is a very non-linear change in stiffness. In the new method, this caused that the first hinge just did

not lock soon after the second hinge, although it was almost there. In ADAMS, however, they locked soon after each other. Nevertheless, the same frequency behavior and vibration amplitudes are observed. Based on the observation where the 3D model of the new method and ADAMS are compared (see figure 9) and a similar behavior is noticed, it is concluded that apparently the beam-like model and the 3D model yield the same results. It is explained by the rather stiff bodies with high eigenfrequencies.

Figure 9 shows that the new algorithm also works well when the body has more than two interface points. Note that the yoke is modelled with three interface points and the panels have each four interface points. Further, the deployment torques and the lock stiffness are partitioned over the hinges. Comparing figure 8 and figure 9 shows that the new method provides similar results for a beam like reduction and a 3D reduction with more interface points. So the same differences with MSC/ADAMS are found.

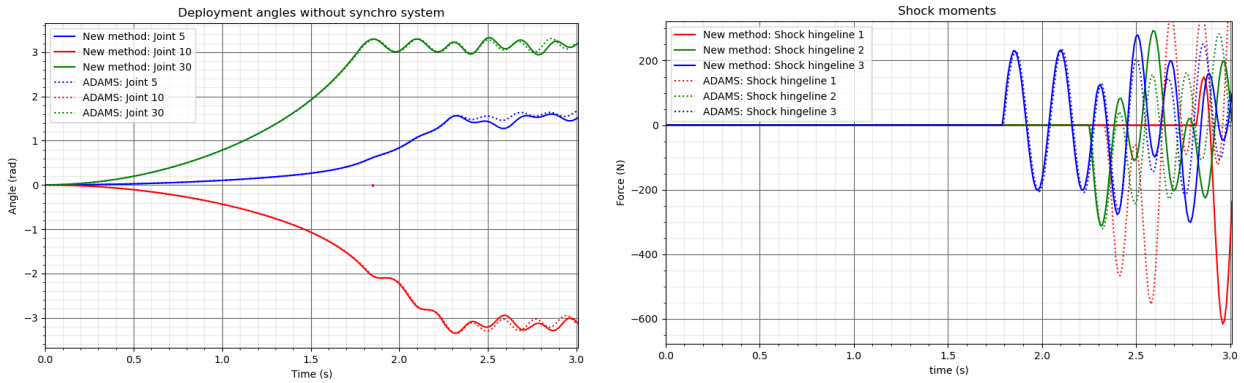

Figure 8: Deployment angles and torques after locking of the unsynchronized beam-like model with two interface points.

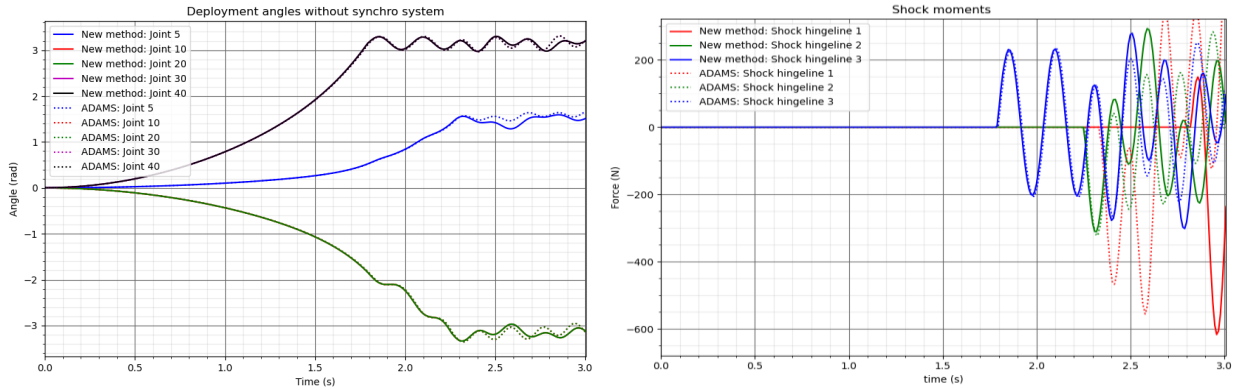

Figure 9: Deployment angles and torques after locking of the unsynchronized 3D model with more than two interface points.

5.2 Synchronized deployment

In this section the synchronized array is studied. Again the results of the new method are compared with the 3D multibody results obtained with MSC/ADAMS. First results from the beam-like model are given. In figure 10 the deployment angles and the shocks are presented and in figure 11 the synchronization forces. Both figures show that the comparison between the new method and MSC/ADAMS are very good. They also show that the angles indeed are synchronized. Apparently, synchronizing the angles takes care that the new method and MSC/ADAMS also compare after locking.

Figures 12 and 13 show that the new algorithm also works very good for the 3D multi body model. The results of the new method and MSC/ADAMS are almost identical. Again, the control has removed the small differences between the new method and ADAMS.

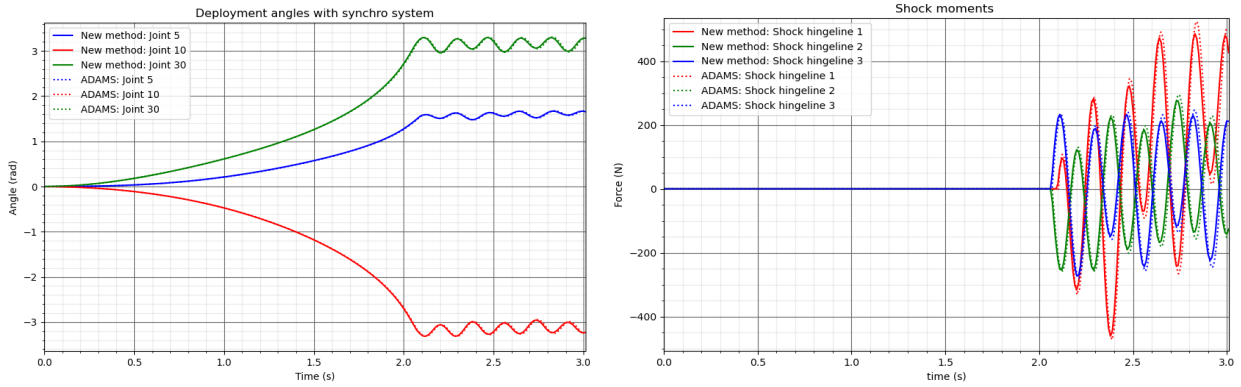

Figure 10: Deployment angles and torques after locking of the synchronized beam-like model with two interface points.

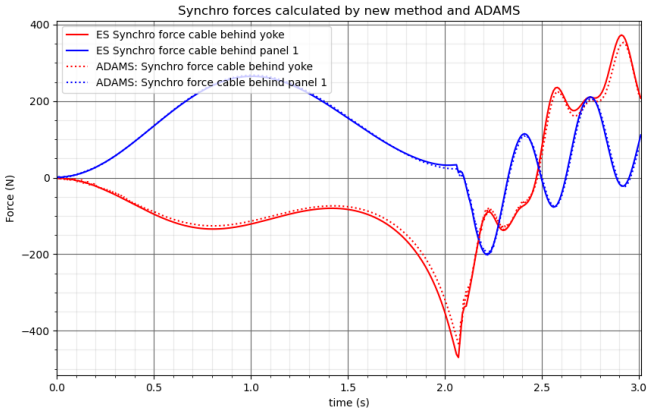

Figure 11: Synchronization torques for the synchronized beam-like model with two interface points.

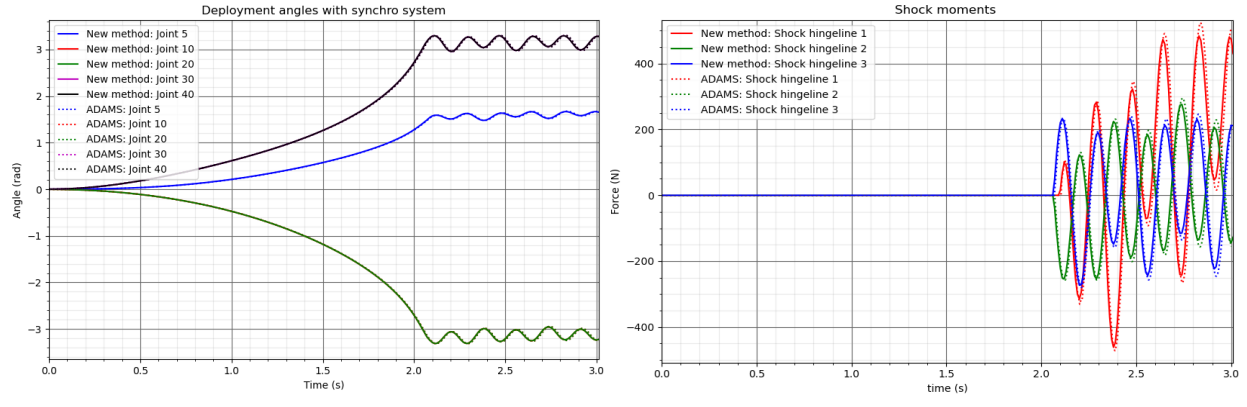

Figure 12: Deployment angles and torques after locking of the synchronized 3D model with more than two interface points.

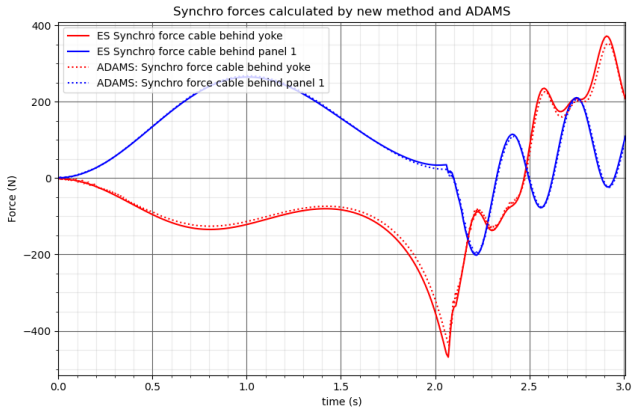

Figure 13: Synchronization torques for the synchronized 3D model with more than two interface points.

To summarize, the results show that the synchronization system works fine. Also it observed that there are no real differences between the model with two interface points and the model with more interface points. This is due to the fact that the bodies are very stiff. Comparison of the results with MSC/ADAMS shows that the new method produces accurate results.

6 Conclusion

A new flexible multibody algorithm was explained. It is obtained by converting the floating frame of reference degrees of freedom to the absolute nodal coordinates. In previous work, it was shown that this new formulation performs very good for bodies with two interface points. This paper shows that the new algorithm also performs very good if the bodies have more than 2 interface points.

As an example the deployment of a solar array was simulated. Two multibody models of the array were created. One model where all bodies had two interface points and a second model where the yoke had three interface points and the panels had four interface points. Two different simulations were run. One without a synchronization system and one with a synchronization system active.

Results obtained without a synchronization system were compared with MSC/ADAMS results, although the ADAMS model was based on bodies with more than two interface points. However, this appeared of no importance because the bodies were modelled rather stiff. The results showed that the new method performs well with more than two interface points.

Next a simulation was run with the synchronization system active. The results showed that the synchronization system worked fine and the angles locked at the same time. Moreover, the results from the new method compared very well with the results from MSC/ADAMS.

To summarize, the new method shows very good results both with beam-like bodies and with bodies having more than two interface points.

References

[1] M.H.M. Ellenbroek, J.P. Schilder, "On the use of absolute nodal coordinates in the floating frame of reference formulation for flexible bodies," *Multibody System Dynamics*, 2017

[2] J.P. Schilder, K.S. Dwarshuis, M.H.M. Ellenbroek and A. de Boer: "The tangent stiffness matrix for an absolute nodal ccordinates floating frame of reference formulation," *Multibody System Dynamics*, 2019

[3] E.J. Haug, *Computer Aided Kinematics and Dynamics of Mechanical Systems, Basic Methods*, Prentice Hall, New York, 1989

[4] A.A. Shabana, *Dynamics of Multibody Systems*, Cambridge University Press, Cambridge, 1998

[5] A. Cardona and M. Géradin, "Modeling of superelements in mechanism analysis," *Int. J. Numer. Methods Eng*, no 32, pp 1565–1593, 1991

[6] Adams - *The Multibody Dynamics Simulation Solution* (https://www.mscsoftware.com/product/adams)

[7] MSC Nastran, *Multidisciplinary Structural Analysis* (https://www.mscsoftware.com/product/msc-nastran)

[8] M.H.M. Ellenbroek and T. Konink, "The non-linear deployment of the solar array wing for the Sentinel 1 satellite," *40th Aerospace Mechanism Symposium*, Cocoa Beach Florida, 2010

[9] M.H.M. Ellenbroek, T. Konink and C. Verheul, "The deployment of the solar array wing for the Sentinel 1 satellite," *ESA Workshop Multi Body Dynamics*, 2010